



Synthesis and Characterization of Lanthanum doped Co-Zn Spinel Ferrites Nanoparticles by Sol-Gel Auto Combustion Method

Zaheer Abbas Gilani¹, Amir Farooq¹, H. M. Noor ul Huda Khan Asghar^{1*}, Muhammad Khalid²

¹ Department of Physics, Balochistan University of Information Technology, Engineering & Management Sciences, Quetta 87300, Pakistan

² Department of Physics, University of Karachi 24700, Pakistan

ARTICLE INFO

Article History:

Received: April 18, 2020

Revised: May 28, 2020

Accepted: June 28, 2020

Available Online: June 30, 2020

Keywords:

Co-Zn ferrite

Spinel ferrites

Nanocrystallite ferrites

Sol-gel

XRD

FTIR

Dielectric properties

ABSTRACT

Spinel ferrites nanoparticles play a significant role in our everyday lives. In the current work, La³⁺ doped Co-Zn ferrites with chemical formula Co_{0.5}Zn_{0.5}La_xFe_{2-x}O₄ (x = 0.00 to x = 0.2 with step size 0.04) was effectively prepared by sol gel technique. The formation of FCC spinel structure was confirmed by X-Ray diffraction (XRD) analysis. The average crystallite size were calculated to be in the 8 nm to 13 nm range. The lattice parameters were found to be decreased with the doping of lanthanum (La³⁺) contents. X- Ray density is analyzed to increase as the concentration of (La³⁺) doping increases, this is due to the fact that La³⁺ ion has a higher molar weight than Fe³⁺ ion. The spinel phase structure was affirmed by using FTIR. The two main absorption bands ν_1 and ν_2 are referred to tetrahedral stretching band and octahedral stretching band respectively, is found to be in the range of at around 400-530 cm⁻¹. Spinel ferrites, such as Co-Zn spinel ferrites, have dielectric features that make them ideal for use in high-frequency applications. With new potential applications being investigated all the time. Physical properties, synthesis method, as well as sintering temperature and time, are all important factors in regulating the properties of dielectric materials. The dielectric features were measured in the frequency of 1 MHz to 3 GHz range. Lowered dielectric parameters studied across a higher frequency range recommend that such nano crystalline ferrites could be used to fabricate the equipment needed to perform at GHz frequencies.



© 2020 The Authors, Published by iRASD. This is an Open Access article under the Creative Common Attribution Non-Commercial 4.0

*Corresponding Author: noorulhudakhan@gmail.com

1. Introduction

The potential and theory of nano science and technology is focused on the fact that materials at the nanoscale have mechanical, chemical, electrical, magnetic, and optical properties that are completely different from bulk materials (Mansoori, 2005). Some of these characteristics are intermediate between those of the smallest constituents (such as particles and atoms) from which they can originate and those of microscopic level materials when contrasted to bulk materials. As nanoparticles are used in comparative applications, it shows that they have execution abilities. Nanotechnology has a wide range of current and future applications, including bottom-up approaches in medicine, genetics, medicines, electronics, electricity, and the environment (Mansoori & Soelaiman, 2005). A stainless steel substance with magnetic characteristics which can be used in a wide variety of devices. Ferrites are stiff, porous, metal, grey or black in color, and poly - crystalline, made up of several smaller clusters. Ferrites are made up of a specific mixture of Fe₂O₃ and one

or more elements. The discovery of stones with an inclination to iron hundreds of years preceding the Christ's birth began the history of ferrites. The massive wedge of these rocks was discovered in Magnesia. These are being used as solvents in paintings at some stage during the Paleozoic era. Ferrites have the general formula $MeFe_2O_4$ and Me is a divalent metal ion in this case. The interconnected arrangement of covalently bonded oxygen anions and metallic ions is known as the ferrite structure. Ferrites are commonly thought of as having a high tensile strength when compared to metals (Matsushita et al., 2006). The most widely used ferrites are the spinel ferrites. Spinel ferrites are an amazing family of oxides that modify the pattern of typical spinel ferrites (Hill, Craig, & Gibbs, 1979). Although a few mechanically significant spinels are organic, magnetite with general formula Fe_3O_4 is a characteristic oxide that is still one of the most important and perhaps the most known with useful applications. Spinel ferrites are ionic in nature. Numerous aspects, including covalent-bonding impact and metal oxide cation crystalline lattice normalization energies, influence cation adherence to specific sites. The crystal structures of spinel ferrites with a net charge of 8, various types of cations sorting can occur to even out the anion's net negative charge (Verweel & Smit, 1971). Spinel crystal structure was first discovered by Bragg (Bragg, 1915) and Nishikawa (Nishikawa, 1915) in 1915. The crystal structure of spinel ferrites with general formula AB_2O_4 . The atoms of oxygen are arranged in a cubical arrangement, where A and B represents tetrahedral and octahedral sites of the crystal structure of spinel ferrites. The domain class Fd_3m is found in the majority of spinel compositions. $M_8Fe_{16}O_{32}$ is the formula, overall the oxygen anions in the cubic unit cell make up 96 interstitial spaces, and 64 and 32 A and B lattice sites.

The cubic spinel structure ferrites unit-cell is moulded with 56 atoms and 32 of those are oxygen atoms, which are arranged in a cubic near stuffed structure, with 24 transition metals spread among 8 lattice site A and 16 lattice site B. Completely accessible There were 64 A lattice sites, but only 8 are involved, and there are 32 accessible B lattice sites, but only 16 were involved to charge neutrality. Spinel crystal structure can be categorized into regular, inverse, or intermediate spinel ferrites based on cation distribution between these A and B lattice sites. For regular spinel inversion parameter = 1, for inverse spinel inversion parameter = 0, and for intermediate ferrite δ ranges varies among these two acute ranges (Sickafus, Wills, & Grimes, 1999). In spinel ferrites, not all interstitial sites are the same; lattice sites A are connected by four oxygen ions that are closest to each other. As a result, lattice sites A are referred to as tetrahedral sites. A tetrahedral site is formed by three atoms in a field contacting one another, with a fourth atom sitting on top in a trigonal arrangement. To maintain charge neutrality in the crystal structure, only 8 of the 64 A lattice sites are involved. The interstitial sites in octahedral lattice sites B in cubic spinel crystal structure are formed by the coordination of 6 closest oxygen particles. The sides of an octahedron are present in the oxygen particles at the lattice site B. 4 of the six particles are in a line, while the other two are in the trigonal position above and below the plane. Only 16 of the 32 lattice sites B in a crystal structures are filled to maintain charge neutrality (Smit, Wijn, & Ferrites, 1961).

In the present study, we have developed a Co-Zn ferrites series by substitution of La^{3+} using the sol-gel method. We studied the different structural and dielectric properties by changing the concentration.

2. Experimental Procedure

Lanthanum substituted Cobalt-Zinc spinel ferrites with chemical formula $Co_{0.5}Zn_{0.5}La_xFe_{2-x}O_4$ ($x = 0.00, 0.04, 0.08, 0.12, 0.16, 0.20$) were effectively prepared by using Sol-Gel technique. Where x denotes varying proportion of impurity doped that is La^{3+} . The chemicals used were Cobalt (II) Nitrate Hexa-Hydrate [$Co(NO_3)_2 \cdot 6H_2O$] M.W = 291.03 made by Sigma-Aldrich, (99%), Zinc Nitrate [$Zn(NO_3)_2 \cdot 6H_2O$] M.W = 297.46, Lanthanum Nitrate [$La(NO_3)_3 \cdot 6H_2O$] M.W = 433.02 made by Merck-Germany (99.9%), Iron Nitrate [$Fe(NO_3)_3 \cdot 9H_2O$] M.W = 404 made by GPR and Citric Acid [$C_6H_8O_7 \cdot H_2O$] (99.9%). The solutions of the samples were prepared in order to make the homogeneous mixture and magnetic stirrer rod was used to dissolve chemicals properly in distilled water. After preparation and properly mixing of solution proportionate forms of solutions in six different beakers were put it on the hotplate. To increasing the temperature between (90°C-120°C) for up to 2 Hours. The materials inside the beakers are subjected to form Gel at the bottom, which contributes to the formation of Sol with the consistent increase in temperature. The

samples were burned due to increase in temperature to 200°C. The burned samples are subjected to properly grinded one by one in such a way that the Samples became in the form of fine powder. After the samples were properly grinded, Hydraulic press was used for pelleting by applying 07 Ton compressed forced. After annealing the specific amount of the materials were taken out and make pellets for each samples by Hydraulic press to applying 07 Ton of force. After making the pellets the remaining samples are put into different tubes. Different characterization techniques, such as XRD, FTIR, Dielectric, SEM etc., were used to characterize the materials.

3. Results and Discussion

3.1. XRD Analysis

The X-ray diffraction pattern for all $\text{Co}_{0.5}\text{Zn}_{0.5}\text{La}_x\text{Fe}_{2-x}\text{O}_4$ ($x = 0.0, 0.04, 0.08, 0.12, 0.16, 0.2$) spinel ferrite nano particles synthesized via sol-gel technique. The Co-Zn composites samples were sintered for 5 hours at 700°C. The crystal structure and crystalline phase pattern was identified using the XRD. Which is a very helpful method for calculating crystalline parameters. The XRD most intense peak was reported at $2\theta = 35^\circ$, which is usually assumed to be an optimal intense peak for cubic crystal structure. All of the peaks are well matched with the peak of Co-Zn ferrite recorded in JCPDS card number # 22-1086 and are listed respectively as (220), (311), (400), (422), (511), (440), (620) and (622). The positions and miller indices of the peaks show that a FCC spinel structure has formed. The FCC spinel structure is described by all of the peaks in the pattern, suggesting that the prepared ferrites had an FCC spinel structure. Some impurity peaks obtained at $2\theta = 33^\circ$, the presence of these impurity peaks revealed that La^{3+} was insoluble in the octahedral site (Gilani et al., 2015). The XRD pattern shown in Figure 1. The Debye Scherrer formula was used to determine the average crystallite size (D_m), given as:

$$D_m = \frac{k\lambda}{\beta \cos\theta} \quad (1)$$

Where $k = 0.9$ for spinel ferrites, $\lambda = 1.54 \text{ \AA}$ represents the x-ray beam wavelength, ' β ' is the FWHM of the most intense peak and θ is the angle of the diffraction of the most intense peak. The crystalline size was measured to be in 8 nm to 13 nm range, and was found to be very small. The size of the crystallites increases as the concentration of La^{3+} doping increases to be in the range of 8 nm ($x=0.0$) to 13 nm ($x=0.20$) [9,10].

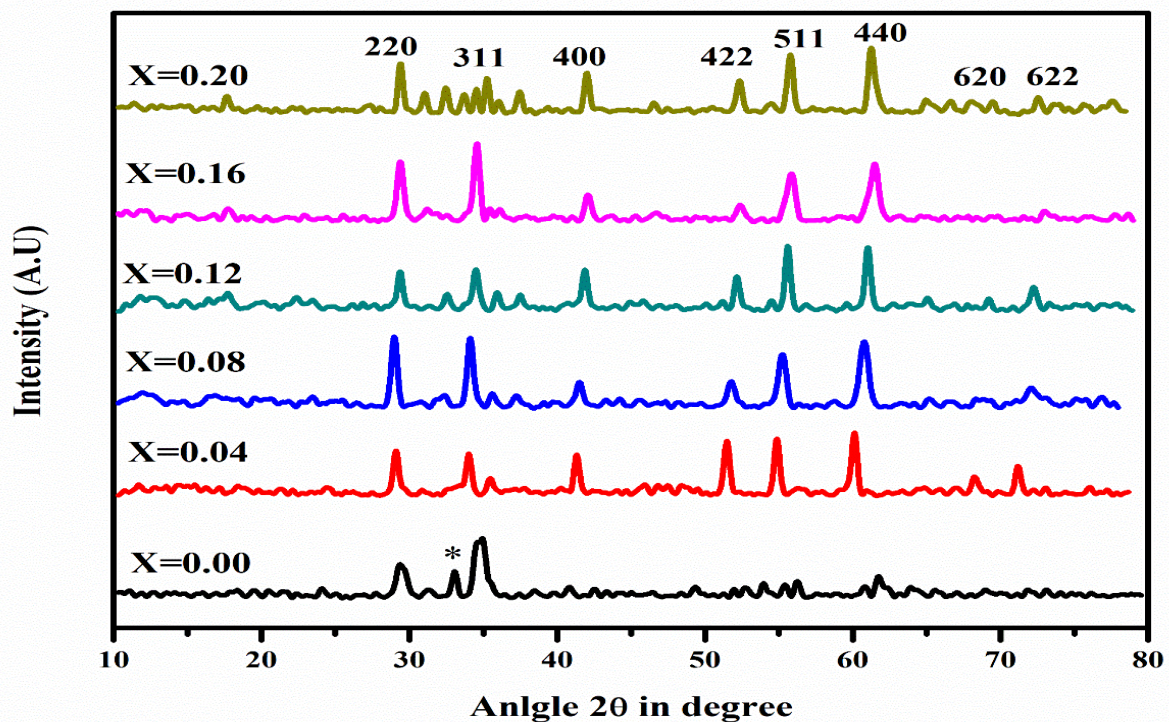


Figure. 1. XRD analysis of La^{3+} doped Co-Zn ferrites ($x = 0.00$ to $x=0.20$ with step size $x = 0.04$)

The average lattice parameter 'a' can be calculated by the following formula given as:

$$a = d\sqrt{h^2 + k^2 + l^2} \quad (2)$$

Where 'd' is the crystal planes spacing and hkl represents the values of miller indices. The average lattice constant was measured for all samples to be in the range of 8.49 Å to 8.56 Å. The ionic radii of the ions La^{3+} and Fe^{3+} were being used to explain the average lattice parameter 'a'. The average lattice parameter was found to be decreased with the La^{3+} doping contents (Mustafa et al., 2020). X-ray density ρ_x can be measured by using the following formula:

$$\rho_x = \frac{8M}{Na^3} \quad (3)$$

Where 'M' is the composition molecular weight, Z=8 for spinel structure represent the number of molecules per unit cell, N is the Avogadro No. (6.0221×10^{23}) and a^3 is a volume of the unit cell. X-Ray density was calculated in the range of 5.06 g/cm³ to 5.51 g/cm³. The relation between X-Ray density and concentration, the curve is almost linear, which mean the X-Ray density increases as the amount of La^{3+} doping increases, Because La^{3+} has a stronger molar weight than Fe^{3+} (Sheikh et al., 2019). The Bulk density by size and mass of the pellets can be determined by using the following relation:

$$\rho_m = \frac{m}{v} \quad (4)$$

Where 'm' represents mass and 'v' represents volume of the pellets. The bulk density were calculated from 2.94 g/cm³ to 3.51 g/cm³ range. The bulk density first increases then decreases and then again increases gradually due to the concentration of La^{3+} doping. Consequently, the reduction in bulk density corresponds to the overall weight of pallets (Khalid et al., 2021). The lattice strain is calculated by using the following formula:

$$\varepsilon = \frac{\beta}{4\tan\theta} (10^{-3}) \quad (5)$$

Where θ is the angle of diffraction of the most intensity peak. Lattice strain was calculated to be in the range of 8.87×10^{-3} to 13.68×10^{-3} . The lattice strain is found to be decreases as the amount of La^{3+} doping increases. The higher value of lattice strain was observed at the value of $x = 0.0$. Micro-strain can be determined by using the following relation given as:

$$\text{Micro - strain} = \frac{\beta\cos\theta}{4} (10^{-3}) \quad (6)$$

Micro-strain was calculated to be in the range of 2.66×10^{-3} to 4.11×10^{-3} . The micro-strain is found to be decreases as the concentration of La^{3+} doping increases. The higher value of micro-strain was observed at the value of $x = 0.0$. Dislocation density of the prepared nanoparticles can be determined by using the following equation given as:

$$\delta = \frac{1}{D^2} (10^{15}) \quad (7)$$

Where 'D' is the crystalline size. The Stacking fault of the prepared ferrites can be determined by using the following relation given as:

$$\text{Stacking Fault (SF)} = \frac{2\pi^2}{45\sqrt{3}\tan\theta} \quad (8)$$

The Stacking Fault was calculated to be in the range of 0.4510 to 0.4538. The stacking fault first increases then gradually decreases which may be due to the concentration of La^{3+} doping. The maximum value of stacking fault is found to be at the value of $x = 0.04$. Table 1 shows the different structural parameters of XRD analysis with different doping concentration

Table 1**Different parameters for crystal composition of La³⁺ doped Co-Zn ferrites (x= 0.00 to x=0.20 with step size x= 0.04)**

Parameters	x = 0.0	x = 0.04	x = 0.08	x = 0.12	x = 0.16	x = 0.20
Crystalline size (nm)	8.435	10.267	10.021	11.096	11.398	13.009
Lattice constant a(Å)	8.545	8.566	8.556	8.525	8.495	8.492
Cell volume (a ³)	624.006	628.573	626.333	619.659	613.126	612.392
X-Ray density (gram/cm ³)	5.0635	5.0969	5.1856	5.3127	5.4413	5.5199
Bulk density (gram/cm ³)	2.947	3.352	3.449	3.159	3.144	3.512
Lattice-Strain (10 ⁻³)	13.683	11.554	11.641	10.442	10.182	8.870
Micro-strain (lines ⁻² /m ⁻⁴) (10 ⁻³)	4.108	3.375	3.458	3.123	3.0399	2.663
Dislocation-density (lines/m) (10 ¹⁵)	14.055	9.486	9.958	8.122	7.697	5.909
Stacking fault	0.451	0.454	0.4536	0.452	0.4523	0.4509

3.2. FTIR Spectroscopy

We used FTIR to confirm the spinel phase structure of all the samples. We learned about cations distribution in all sites (tetrahedral and octahedral) in a crystal from FTIR, as well as chemical changes in the composition. In every concentration of Co_{0.5}Zn_{0.5}La_xFe_{2-x}O₄ (x=0.00, 0.04, 0.08, 0.12, 0.16, 0.20) ferrites, the spinel phase structure was affirmed by using FTIR. The features of spinel crystal structure are classified into two primary frequency bands one is high frequency band ν_1 (approx. 500 cm⁻¹) and the other one is the low frequency band ν_2 (approx. 400 cm⁻¹). Because of the tetrahedral site of inherent stretching vibration, the absorption peaks are referred to as higher frequency bands ν_1 . The term "lower frequency bands ν_2 " refers to octahedral stretching bands. The FTIR spectra are shown in Figure 2 was ranged between 400 to 1000 cm⁻¹. The table shows the various frequencies that can be achieved by increasing the La³⁺ content (Gilani et al., 2015). The higher frequency bands ν_1 varied from 535 to 544 cm⁻¹ whereas in the lower frequency bands ν_2 values remain same which shows that the frequency band remain static. The strength of absorption bands ν_1 and ν_2 changes due to the difference in stretching vibrations of Fe³⁺- O²⁻ at tetrahedral lattice sites and octahedral lattice sites.

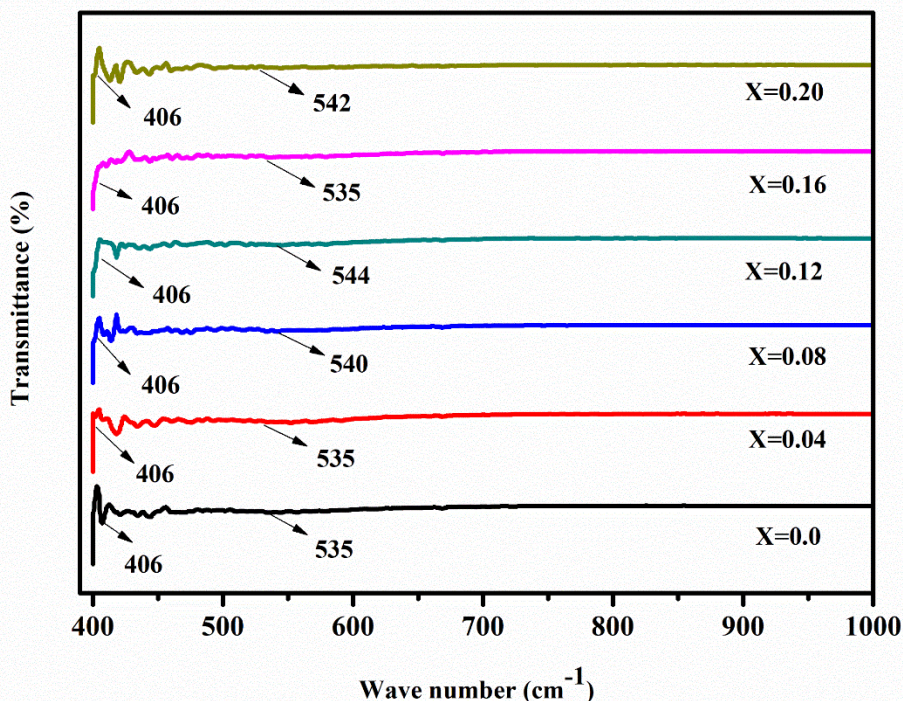


Figure 2. FTIR spectra of La³⁺ doped Co-Zn ferrites (x= 0.00 to x=0.20 with step size x= 0.04)

Furthermore, Figure 2 shows that as the amount of lanthanum in the nanoparticles increases, the frequency band shifts slightly, which could be due to grain size and lattice parameters. The Fe³⁺-O²⁻ stretching vibrations were caused by changes in lattice constant,

resulting in a shift in band position. Furthermore, when six sets of data are compared, it is revealed that as lanthanum concentration rises, the intensity of the ν_1 absorption band increases as well, whereas the intensity of the ν_2 absorption band remains unchanged (Shahzadi et al., 2020). The values of force constants, denoted by K_t and K_o for tetrahedral and octahedral sites, were computed from Table 2 using the following formulas:

$$K_{octa} = 0.942128 M (\nu_2)^2 / (M+32) \quad (9)$$

$$K_{tetra} = \sqrt{2} K_o \nu_1 / \nu_2 \quad (10)$$

Where ν_1 and ν_2 are high frequency and low frequency bands respectively, M shows the molecular weight of the composition. The values of tetrahedral and octahedral radii were also determined using the following formulas:

$$R_{tetra} = a \sqrt{3} (u - 0.25) - R_o \quad (11)$$

$$R_{octa} = a (5/8 - u) - R_o \quad (12)$$

Where R_{tetra} and R_{octa} represents the tetrahedral and octahedral radii respectively, 'a' is the lattice parameter and 'u' is the oxygen position parameter. For FCC structure the value of oxygen parameters is 0.375. The values of different FTIR parameters were computed in below Table 2.

Table 2
Different structural parameters involved in FTIR spectra

Parameters	x = 0.00	x = 0.04	x = 0.08	x = 0.12	x = 0.16	x = 0.20
Molecular weight (g/mole)	237	241	244	247	251	254
ν_1 /cm ⁻¹	535	535	540	544	535	542
ν_2 /cm ⁻¹	406	406	406	406	406	406
K_{octa} (dyne/cm ²) × 10 ⁵	1.36881	1.37105	1.37323	1.37537	1.37745	1.37949
K_{tetra} (dyne/cm ²) × 10 ⁵	2.55085	2.55502	2.58301	2.60619	2.56696	2.60439
R_{octa}	0.081634	0.082154	0.081899	0.081136	0.080385	0.080299
R_{tetra}	0.0530122	0.0534625	0.0532419	0.0525816	0.0519306	0.0518571

3.3. Dielectric Properties

Table 3
Different dielectric properties of La³⁺ doped Co-Zn ferrites (x= 0.00 to x=0.20)

Parameters	Frequency	x =0.0	x =0.04	x=0.08	x =0.12	x =0.16	x =0.2
Dielectric Constant	1 MHz	5.9822	5.3315	5.5405	5.9616	4.6260	3.9242
	1 GHz	6.2626	5.5560	5.2872	5.3028	4.9767	4.9546
	3 GHz	5.6709	5.28581	4.48815	4.9839	4.34863	4.6512
Dielectric loss	1 MHz	-0.494	-0.921	-0.065	-0.081	-0.198	-0.285
	1 GHz	0.0367	0.1839	0.0281	0.2808	0.0953	0.1844
	3 GHz	0.27442	0.25499	0.11167	0.12388	0.13794	0.12857
Tangent loss	1 MHz	-0.0827	-0.1728	-0.0118	-0.01375	-0.0428	-0.0726
	1 GHz	0.0058	0.03311	0.0053	0.05297	0.0191	0.0372
	3 GHz	0.04839	0.04824	0.02488	0.02486	0.03172	0.02764
AC Conductivity	1MHz	2.56298	1.64593E	3.07773	5.77269E	7.79359E	2.41441
		E-05	-05	E-05	-05	-06	E-05
	1GHz	0.00148	0.011194	0.00156	0.010787	0.004610	0.00930
		6	1			3	
	3 GHz	0.04398	0.035354	0.02097	0.024476	0.027272	0.02264
		8		7		2	72

Spinel ferrites, such as Co-Zn spinel ferrites, have dielectric features that make them ideal for use in high-frequency instruments, and new applications are being investigated all the time. Physical properties, synthesis method, as well as sintering temperature and time, are all important factors in regulating the properties of dielectric materials. The dielectric features such as dielectric constant, permit loss, PermitTan, Real and Imaginary components of impedance, electric modulus and AC conductivity of La-doped Co-Zn spinel ferrites having chemical formula $Co_{0.5}Zn_{0.5}La_xFe_{2-x}O_4$ (x=0.0, 0.04, 0.08, 0.12, 0.16, and

0.20) were measured in the 1 MHz to 3 GHz frequency range in the present work (Junaid et al., 2016) and are interpreted in the Table 3.

3.3.1. Dielectric Constant and Dielectric Loss

Dielectric constant (ϵ') and dielectric loss (ϵ'') can be calculated by using the formulas given as:

$$\epsilon' = \frac{t}{\omega A \epsilon_0} \times \frac{Z''}{(Z'^2 + Z''^2)} \quad (13)$$

$$\epsilon'' = \frac{t}{\omega A \epsilon_0} \times \frac{Z'}{(Z'^2 + Z''^2)} \quad (14)$$

Where t is the thickness of pellets, 'A' is the area of the pellets surface, ' ω ' is the angular frequency, ϵ_0 is the permittivity of free space (8.85×10^{-12}), Z' and Z'' are the real and imaginary impedance respectively.

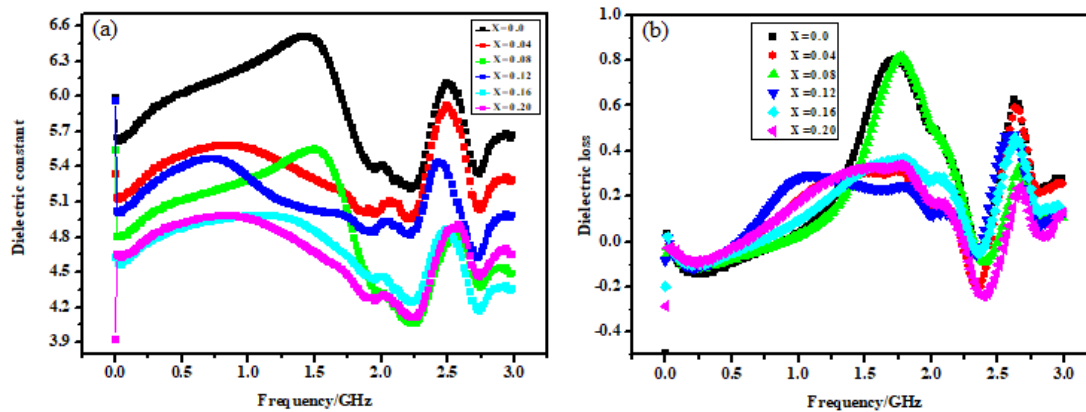


Figure 3: (a) Dielectric constant vs. Frequency graph (b). Dielectric loss vs. Frequency graph

Figure 3(a) shows the dielectric constant graph for the frequency range of 1 MHz to 3 GHz, with various concentrations of La^{3+} . The results showed that the dielectric constant rises with increasing the doping of La^{3+} . It decreases precipitously for all composition in the lower frequency region with increasing the frequency. Dispersion is caused by a decrease in dielectric constant with increasing frequency, which occurs as a function of the applied field at lower frequencies. The inter-facial polarization assumed by the Maxwell-Wagner model can be used to describe dielectric dispersion in ferrites. Ferrites have a dielectric structure with good conducting grains isolated by weak conductor grain boundary. Electron hopping between Fe^{3+} and Fe^{2+} causes electrons to pile up at grain boundaries, causing polarization in ferrites (Khan et al., 2020). Consequently, at low frequencies, electrons hoping between equivalent atoms ions ($\text{Fe}^{3+}-\text{Fe}^{2+}$) generates strong polarization and thus increases the dielectric constant. Furthermore, as the electrons' hoping frequency is gradually increased, the electrons' exchange rate decreases, and the dielectric constant value decreases as well. Dielectric loss in ferrites is primarily caused by electron hopping and defect dipoles. Electron hopping causes dielectric loss only at very low frequencies. The effect of electron hopping decreases with increasing frequency, and thus the dielectric loss in the high frequency field decreases, Figure 3(b) depicts it. Charged distortion dipoles lead to dielectric loss in the high frequency range. The dielectric loss also has a peaking pattern, as shown in Figure 3(b) (Malik et al., 2014).

3.3.2. Tangent Loss and AC Conductivity

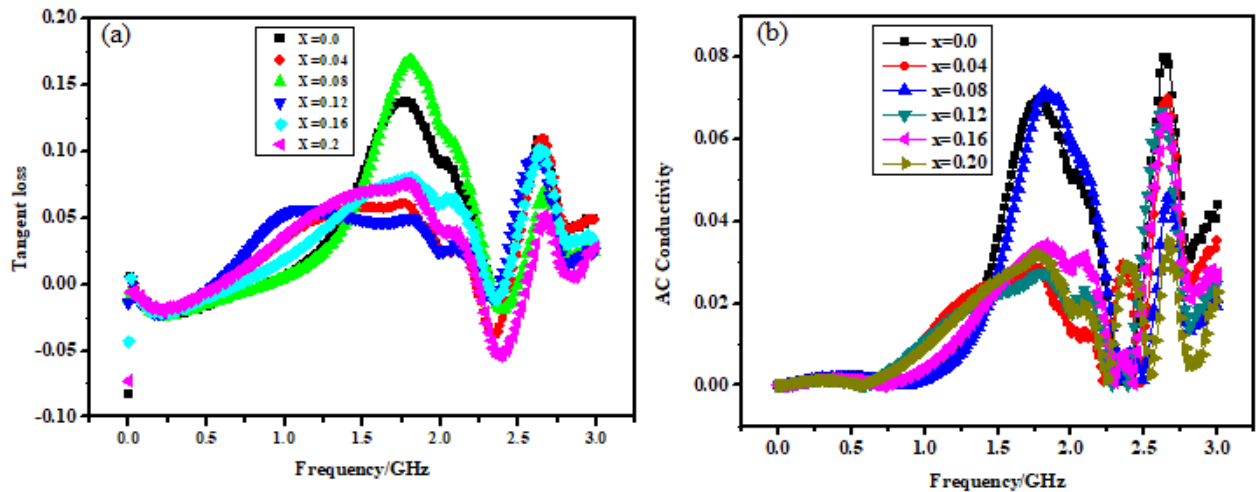


Figure 4: (a) Tangent loss as a function of Frequency (b). AC conductivity as a function of Frequency

The tangent loss (\tan) specifies the rate of energy loss in dielectric materials. The tangent loss (\tan) can be calculated using the formula below:

$$\tan\delta = \frac{\epsilon''}{\epsilon'} \quad (15)$$

Figure 4(a) depicts the tangent loss variance for frequencies ranging from 1 MHz to 3 GHz with various La^{3+} concentrations. It has been seen that the dielectric constant decreases as the applied frequency rises. Permittan is greatest when the applied AC electric field is smaller than the hopping frequency, however, it is minimal when the electrons' hopping frequency is so high that they do not follow the applied Electric field. Permittan is high at low frequencies, as seen in Figure 4(a), and it exponentially decreases as frequency is increased. The low tangent loss of nanoferrites is significant in a variety of applications (Parveen et al., 2019). One of the most important properties of dielectric materials is AC conductivity. At room temperature, the AC conductivity of prepared ferrites of La^{3+} doped Co-Zn ferrites ($x= 0.00$ to $x=0.20$ with step size $x= 0.04$) with respect to frequency from 1 MHz to 3 GHz range can be calculated by the following formula:

$$\sigma_{ac} = \frac{t}{A} \times \frac{Z''}{(Z'^2 + Z''^2)} \quad (16)$$

Where t represents the thickness of the pellets, A represents the pellets surface area, and Z' and Z'' represent the real and imaginary parts of impedance, respectively. In Figure 5 the graph exhibit the dispersion at higher frequency region. The conductivity of all materials is minimal at low frequencies region. Thin conducting grain-barrier layers separated the grains in spinel ferrites. The AC conductivity is influenced by the resistive behaviour of grain boundaries. Figure 4(b) depicts, the minimal AC- conductivity in the low frequency range can be due to the higher resistance of the grain-boundaries, because of charge carrier exchange (hopping) between Fe^{2+} and Fe^{3+} ions at octahedral sites, the grains are conductive in the high frequency field. As a result, the hopping frequency rises as the applied electric field frequency rises, and the AC conductivity rises (Mustafa et al., 2020).

3.3.3. Real and Imaginary Impedance

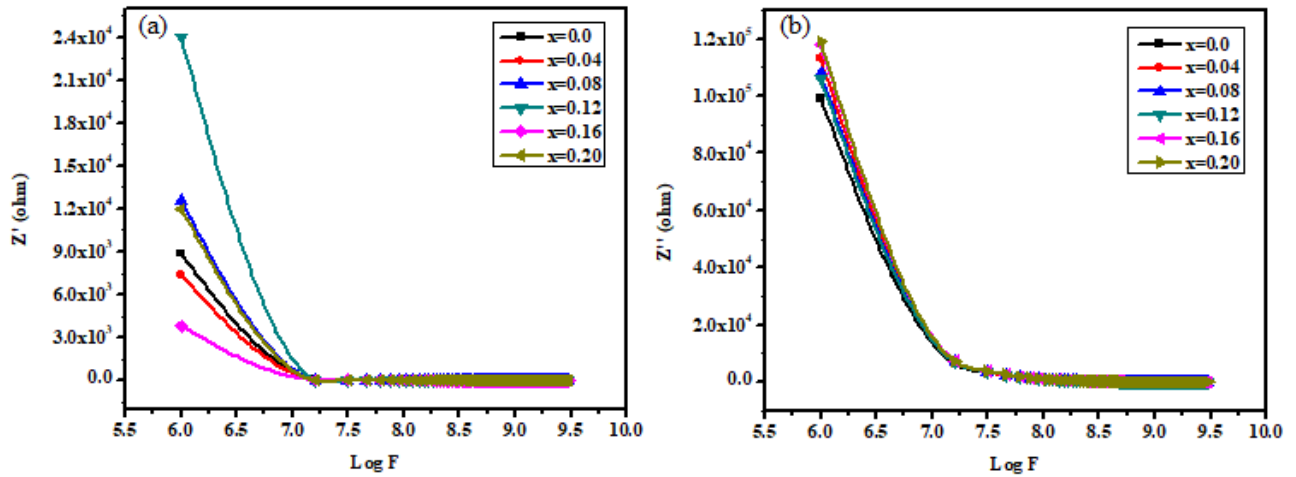


Figure 5(a). Real parts of impedance as a function of Log F (b). Imaginary parts of impedance as a function of Log F

The applied frequency has a large impact on real and imaginary components of impedance. Figure 5(a) and Figure 5(b) depict the impedance with respect to frequency from 1 MHz to 3 GHz range. The following relations can be used to determine real impedance (Z') and imaginary of impedance (Z'')

$$Z' = R = |Z| \cos\theta_z \tag{17}$$

$$Z'' = X = |Z| \sin\theta_z \tag{18}$$

The resistive behaviour of grain barriers due to inter-facial polarization is recorded in the low-frequency region for all compositions, resulting in a high impedance. Impedance analysis is showing the real and imaginary impedance decrease with increasing the applied frequency and impedance curves merge with each other at high frequency region, because of the conductive behaviour of grains in the higher-frequency field, the impedance is quite low (Khalid et al., 2021; Mustafa et al., 2020).

3.3.4. Real and Imaginary Electric Modulus

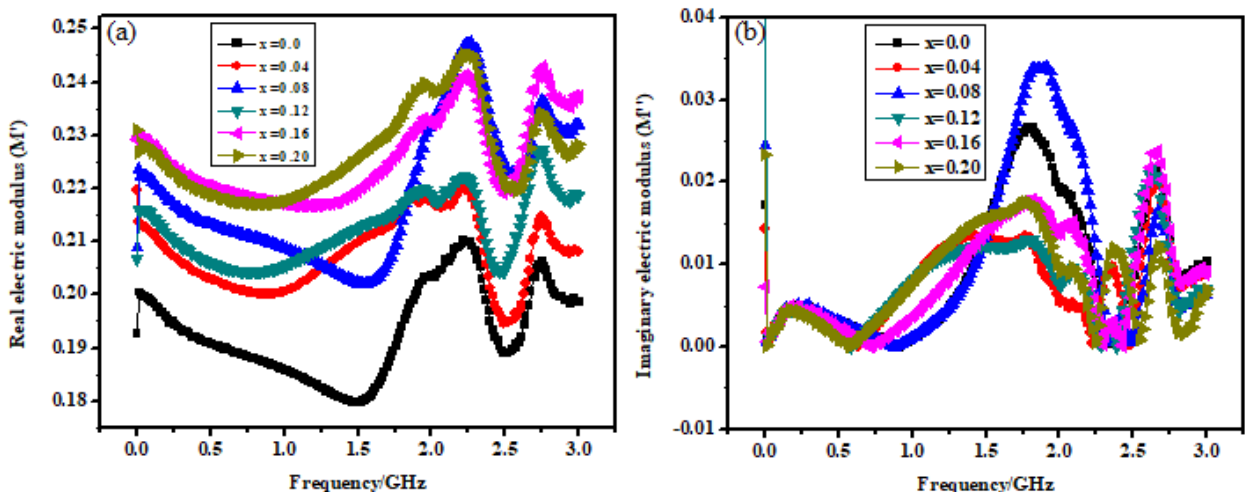


Figure 6: (a)Real electric modulus as a function of frequency (b). Imaginary electric modulus vs frequency

The electric modulus has an effect on the dielectric properties of a material. Modulus features are used to investigate the role of grains and grain barriers in a particular frequency range. Charge carrier and stimulation behaviour of spinel ferrites can be studied using the electric modulus. The real and imaginary parts of the electric modulus in the frequency region of 1 MHz to 3 GHz were calculated using the formulas below:

$$M' = \varepsilon' / (\varepsilon'^2 + \varepsilon''^2) \quad (19)$$

$$M'' = \varepsilon'' / (\varepsilon'^2 + \varepsilon''^2) \quad (20)$$

Where ε' is the real dielectric permittivity or dielectric constant and ε'' is the imaginary dielectric permittivity or dielectric loss. Firstly, the real and imaginary components of the electric modulus have quite lower values in the low-frequency field. Electric modulus analysis is showing the real and imaginary parts of electric modulus increase with increasing the frequency of applied field, while the electric modulus become maximum at high frequency region (Khalid et al., 2021; Mustafa et al., 2020). The different calculated values of impedance and electric modulus are depicted in Table 4.

Table 4
Impedance, Modulus and AC conductivity of La³⁺ doped Co-Zn ferrites (x=0.00 to x=0.20 with step size x=0.04)

Parameters	Frequency	x = 0.00	x = 0.04	x = 0.08	x = 0.12	x = 0.16	x = 0.2
Z' (ohm)	1MHz	8.87E+03	7.38E+03	1.26E+04	2.40E+04	3.79E+03	1.20E+04
	1GHz	4.69E-01	4.13E+00	6.22E-01	4.17E+00	1.99E+00	4.03E+00
	3 GHz	1.79E+00	1.58E+00	1.16E+00	1.20E+00	1.58E+00	1.21E+00
Z'' (ohm)	1MHz	9.92E+04	1.13E+05	1.08E+05	1.06E+05	1.18E+05	1.19E+05
	1GHz	9.51E+01	1.03E+02	1.07E+02	1.05E+02	1.11E+02	1.11E+02
	3 GHz	3.41E+01	3.57E+01	3.98E+01	3.75E+01	4.07E+01	3.92E+01
M'	1MHz	0.192625	0.219643	0.208866	0.206758	0.229126	0.231046
	1GHz	0.185804	0.200621	0.208731	0.205496	0.217077	0.217571
	3 GHz	0.198598	0.2081701	0.232129	0.2186862	0.2373542	0.2282571
M''	1MHz	0.017229	0.014332	0.024463	0.046607	0.007361	0.023403
	1GHz	0.000916	0.008065	0.001215	0.008154	0.003884	0.007881
	3 GHz	0.010423	0.009196	0.006778	0.007099	0.009218	0.007076

4. Conclusions

Spinel ferrites nanoparticles play a significant role in our everyday lives and used in variety of application such as medical industries, nano electronics, and waste water treatment etc. Lanthanum (La³⁺) substituted Co-Zn nanoferrites with general formula Co_{0.5}Zn_{0.5}La_xFe_{2-x}O₄ (x = 0.00 to x = 0.20 with step size 0.04) was effectively synthesized via sol-gel technique, that is the easiest way to synthesis of such types of nano ferrites. The XRD process was used to examine crystal structure and crystalline phase formation, which is a very helpful method for calculating crystalline features such as crystalline size, lattice constant, lattice strain, micro-strain, X-ray density, bulk density and stacking fault. The XRD most intense peak was reported at 2θ=35°, which is usually assumed to be an optimal intense peak for cubic crystal structure. The positions and miller indices of the peaks show that a FCC spinel structure has formed. The spinel phase structure was affirmed by using FTIR. The features of spinel structure are classified into two primary frequency bands one is the higher frequency band ν_1 (approx. 500 cm⁻¹) and the other one is the lower frequency band ν_2 (approx. 400 cm⁻¹). Because of the tetrahedral site of inherent stretching vibration, the absorption peaks are referred to as higher frequency bands ν_1 . The term "lower frequency bands ν_2 " refers to octahedral stretching bands. Spinel ferrites, such as Co-Zn spinel ferrites, have dielectric features that make them ideal for use in high-frequency instruments, and new applications are being investigated all the time. Physical properties, synthesis method, as well as sintering temperature and time, are all important factors in regulating the properties of dielectric materials. The dielectric properties of La-doped Co-Zn spinel ferrites were measured in the frequency of 1 MHz to 3 GHz range. The lowered dielectric features identified across a higher frequency range recommend that such nano - crystalline ferrites could be used to fabricate the equipment needed to perform at GHz frequencies.

Acknowledgement

We are grateful to ORIC of Balochistan University of Information Technology, Engineering and Management Sciences (BUIEMS), Quetta Pakistan.

Reference

- Bragg, W. H. (1915). XXX. The structure of the spinel group of crystals. *The London, Edinburgh, and Dublin Philosophical Magazine and Journal of Science*, 30(176), 305-315.
- Gilani, Z. A., Warsi, M. F., Khan, M. A., Shakir, I., Shahid, M., & Anjum, M. N. (2015). Impacts of neodymium on structural, spectral and dielectric properties of LiNiO. 5Fe₂O₄ nanocrystalline ferrites fabricated via micro-emulsion technique. *Physica E: Low-dimensional Systems and Nanostructures*, 73, 169-174.
- Hill, R. J., Craig, J. R., & Gibbs, G. (1979). Systematics of the spinel structure type. *Physics and chemistry of minerals*, 4(4), 317-339.
- Khalid, M., Chandio, A. D., Akhtar, M. S., Khan, J. K., Mustafa, G., Channa, N. U., & Gilani, Z. A. (2021). Aluminum Substitution in Ni-Co Based Spinel Ferrite Nanoparticles by Sol-Gel Auto-Combustion Method. *Journal of Electronic Materials*, 50(6), 3302-3311.
- Khan, J. K., Khalid, M., Chandio, A. D., Shahzadi, K., Uddin, Z., Mustafa, G., . . . Gilani, Z. A. (2020). Properties of Al³⁺ substituted nickel ferrite (NiAl_x Fe_{2-x} O₄) nanoparticles synthesised using wet sol-gel auto-combustion. *Journal of Sol-Gel Science and Technology*, 1-12.
- Malik, H., Mahmood, A., Mahmood, K., Lodhi, M. Y., Warsi, M. F., Shakir, I., . . . Khan, M. A. (2014). Influence of cobalt substitution on the magnetic properties of zinc nanocrystals synthesized via micro-emulsion route. *Ceramics International*, 40(7), 9439-9444.
- Mansoori, G. A. (2005). *Principles of nanotechnology: molecular-based study of condensed matter in small systems*: World Scientific.
- Mansoori, G. A., & Soelaiman, T. F. (2005). Nanotechnology—an introduction for the standards community. *Journal of ASTM International*, 2(6), 1-22.
- Matsushita, N., Kondo, K., Yoshida, S., Tada, M., Yoshimura, M., & Abe, M. (2006). Ni-Zn ferrite films synthesized from aqueous solution usable for sheet-type conducted noise suppressors in GHz range. *Journal of electroceramics*, 16(4), 557-560.
- Mustafa, G., Khalid, M., Chandio, A. D., Shahzadi, K., Uddin, Z., Khan, J. K., . . . Gilani, Z. A. (2020). Dielectric, impedance, and modulus spectroscopic studies of lanthanum-doped nickel spinel ferrites NiLa_x Fe_{2-x} O₄ nanoparticles. *Journal of Sol-Gel Science and Technology*, 1-10.
- Nishikawa, S. (1915). Structure of some crystals of spinel group. *Proceedings of the Tokyo Mathematico-Physical Society. 2nd Series*, 8(7), 199-209_191.
- Parveen, A., Khalid, M., Gilani, Z. A., Aslam, S., Saleem, M., Shaikh, F. A., & Rehman, J. (2019). Dielectric, impedance and modulus spectroscopic studies of Co_{0.3} Cd_{0.7} Zn_{1.5} x Fe_{2-x} O₄ nanoparticles. *Applied Physics A*, 125(10), 1-11.
- Shahzadi, K., Chandio, A. D., Mustafa, G., Khalid, M., Khan, J. K., Akhtar, M. S., & Gilani, Z. A. (2020). Impact of aluminum substitution on the structural and dielectric properties of Ni-Cu spinel ferrite nanoparticles synthesized via sol-gel route. *Optical and Quantum Electronics*, 52(4), 1-17.
- Sheikh, F. A., Khalid, M., Shifa, M. S., Aslam, S., Perveen, A., ur Rehman, J., . . . Gilani, Z. A. (2019). Effects of bismuth on structural and dielectric properties of cobalt-cadmium spinel ferrites fabricated via micro-emulsion route. *Chinese Physics B*, 28(8), 088701.
- Sickafus, K. E., Wills, J. M., & Grimes, N. W. (1999). Structure of spinel. *Journal of the American Ceramic Society*, 82(12), 3279-3292.
- Smit, J., Wijn, H., & Ferrites, L. (1961). Bibliothèque Technique Philips. *Dunod, Paris*.
- Verweel, J., & Smit, J. (1971). Ferrites at radio frequencies. *Magnetic Properties of Materials*(13), 64.